A robust FWI gradient for high-resolution velocity model building

Jaime Ramos-Martinez*, Sean Crawley, Zuihong Zou, Alejandro Valenciano, Elena Klochikhina and Nizar Chemingui, PGS

Summary

We describe a robust method to produce long-wavelength updates in gradient-based Full Waveform Inversion (FWI). The gradient is computed by applying dynamic weights in the velocity sensitivity kernel derived from impedance and velocity parameterization of the classical objective function. The new kernel implementation effectively eliminates the migration isochrones produced by the specular reflections and emphasizes the low-wavenumber components in the gradient in heterogeneous media. The new gradient is able to provide velocity updates beyond penetration depth of diving waves. We use a synthetic example to illustrate how this dynamically weighted FWI gradient successfully recovers the background velocity from pre-critical reflections. We apply the new approach to 2D and 3D dual sensor data from deep-water Gulf of Mexico. Results show how the dynamically weighted FWI gradient can combine both transmitted and reflected energy in a global   FWI scheme and provide high-resolution velocity models without migration imprint in the updates.

Introduction

In shallow water scenarios, there have been many successful case histories of conventional FWI from refracted and turning waves recorded in OBC (e.g., Liu et al., 2011) or towed streamer data (e.g., Zhou et al., 2014). In these scenarios, recorded diving waves allow FWI to resolve small-scale geologic features up to the deepest turning point. For deeper targets, FWI needs to rely on reflected energy to update the model. However, by using conventional gradient computations, unless the recorded reflections have extraordinary low-frequency content, reflections only allow the reconstruction of the high-wavenumber features of the model.

Thus, there have been numerous efforts to reformulate FWI algorithms to include reflected energy for retrieving long-wavelength updates (e.g., Xu et al., 2013; Zhou et al., 2015, Alkhalifah, 2014). The fundamental idea is to compute a gradient in which undesired migration isochrones corresponding to the specular reflection are not present. In most of the approaches currently available, computation of gradient in this case requires twice the modelling realizations compared to those required by conventional FWI (Zhou et al., 2015).

In this work, we propose an approach to separate the low- from the high-wavenumber components in the gradient and thus produce long-wavelength velocity updates at depths greater than the penetration depth of the diving waves, with almost the same cost of conventional FWI. Our approach consists in inserting dynamic weights in the velocity sensitivity kernel derived from an impedance-velocity parameterization (Douma et al., 2010). This eliminates the migration isochrones that dominate the gradient in heterogeneous media. We first introduce the new FWI gradient and provide insight into its physical interpretation. Then, we present a synthetic example that shows its performance in retrieving the background velocity from short spread data. Finally, we show field data examples where we use the new gradient to build high-resolution velocity models from records containing diving waves and reflections without the migration imprint provided by conventional FWI.

Theory

In conventional FWI, we solve a nonlinear inverse problem by iteratively updating the model to minimize an objective function, which is the difference between the modeled seismic data and the recorded field data. This misfit function is generally minimized in a least-squares sense, and the model update is computed as a scaled representation of its gradient. In the case of an isotropic acoustic medium parameterized in terms of bulk-modulus and density (κ, ρ), Tarantola (1984) shows that the gradient depends on the kernels for κ and ρ that can be written as:

$$K_\kappa(\mathbf{x}) = \frac{1}{\kappa(\mathbf{x})}\int \frac{\partial S(\mathbf{x},t)}{\partial t}\frac{\partial R(\mathbf{x},T-t)}{\partial t}dt \text{ and} \quad (1)$$

$$K_\rho(\mathbf{x}) = \frac{1}{\rho(\mathbf{x})}\int \nabla S(\mathbf{x},t)\cdot\nabla R(\mathbf{x},T-t)dt, \quad (2)$$

where $\kappa(\mathbf{x}) = \rho(\mathbf{x})v^2(\mathbf{x})$ is the equation that relates the bulk-modulus to velocity. In Equations 1 and 2, $S(\mathbf{x},t)$ is the source wavefield and $R(\mathbf{x},T-t)$ is the residual wavefield after time reversal. The sensitivity kernel for a particular parameter measures the variation in the misfit function caused by changing that parameter while holding the others fixed (Tromp et al., 2005). Figures 1a and 1b show the sensitivity kernels corresponding to Equations 1 and 2 in a model consisting of a single layer overlying a homogeneous half-space.

Douma et al. (2010) derived sensitivity kernels for a different parameterization consisting of the acoustic velocity and impedance. These sensitivity kernels can be written in terms of Tarantola's bulk and density kernels as:

A robust FWI gradient for high-resolution model building

$$K_v(\mathbf{x}) = K_K(\mathbf{x}) - K_\rho(\mathbf{x}) \quad \text{and} \quad (3)$$

$$K_Z(\mathbf{x}) = K_K(\mathbf{x}) + K_\rho(\mathbf{x}), \quad (4)$$

The impedance kernel (Equation 4) comprises the high-wavenumber components of the velocity field while the velocity kernel (Equation 3) is restricted to low wavenumbers (Luo et al., 2009). The impedance kernel is useful for RTM where a high-resolution model is desirable and the velocity is fixed. In fact, the aim of Douma et al. (2010) was to prove that under severe assumptions in the simplicity of the background medium and faraway from sources and receiver locations, performing RTM imaging from the impedance kernel shown in equation (3), is equivalent to applying the Laplacian filter to the image resulting from a crosscorrelation imaging condition. In this context, Whitmore and Crawley (2012) used the same impedance sensitivity kernel to derive an imaging condition capable of removing the unwanted backscattered noise. The examples presented in their paper, using heterogeneous models, highlighted the importance of dynamically weighting the different components of the impedance kernel to achieve optimal removal of the low-wavenumber artifacts. Figure 1c shows the result of weighting the components from Figures 1a and 1b to produce an RTM impulse response free of back-scattered noise.

On the other hand, the use of the velocity kernel is ideal for FWI where the low-wavenumber components of the gradient are preferred while the high wavenumbers associated with reflections may mislead the inversion. Following the premises of Whitmore and Crawley (2012), an FWI gradient can be derived by dynamically weighting the velocity sensitivity kernel (Equation 3). Their dynamic weights can be adapted to alternatively remove the high wavenumbers from the FWI gradient in a heterogeneous media. By assuming constant density, the new FWI gradient can be derived from equation (3) as:

$$G(\mathbf{x}) = \frac{1}{2A(\mathbf{x})} \left\{ \int_t \left[W_1(\mathbf{x},t) \frac{1}{v^2(\mathbf{x})} \frac{\partial S(\mathbf{x},t)}{\partial t} \frac{\partial R(\mathbf{x},T-t)}{\partial t} \right] dt - \int_t \left[W_2(\mathbf{x},t) \nabla S(\mathbf{x},t) \cdot \nabla R(\mathbf{x},T-t) \right] dt \right\} \quad (5)$$

where the dynamic weights $W_1(\mathbf{x},t)$ and $W_2(\mathbf{x},t)$ are designed to optimally suppress the migration isochrones, and $A(\mathbf{x})$ is the illumination term. Figure 1d is produced using equation 5; it illustrates how the migration isochrone has been removed while the low-wavenumber energy is preserved.

Figure 2a shows the conventional FWI gradient compared to the modified gradient from Equation 5 (Figure 2b) for a model with a linearly increasing velocity with depth. Here,

the modified gradient in Equation 5 removes the migration isochrone but preserves all the low-wavenumber components associated with the diving waves ("bananas") and backscattering ("rabbit ears").

Synthetic Example

In order to test the effectiveness of our approach, we first design a 2D synthetic example consisting of five homogeneous layers (Figure 3). The data has maximum offsets of 4 km so only pre-critical reflections are used in the inversion. The starting velocity model for FWI contained errors up to 100m/s. The inversion was performed on a frequency band of 3-5 Hz. Figures 3b and 3c show the results of the inversion using the conventional FWI gradient and the dynamically weighted FWI gradient. Results from the new FWI gradient are accurate and do not suffer from the high-wavenumber artifacts observed on the conventional FWI update.

Field Data Examples

First, we compare the dynamically weighted FWI gradient with the traditional FWI on field data from deep-water Gulf of Mexico (DeSoto Canyon). The data were acquired with dual-sensor streamers and with a maximum offset of 12 km. The FWI full-power frequency band was 3-7 Hz. No particular mutes or event selection were used; therefore, all recorded data were employed during the inversion. Figure 4a shows an overlay of the initial velocity model on the seismic image. Figures 4b and 4c show the updates from the conventional and the dynamically weighted gradients. As observed, the FWI gradient produces good resolution model updates that are free from high-wavenumber artifacts. Also noticeable is the imprint of the seismic reflectivity on the conventional FWI updates. To further evaluate the model derived from the new gradient, we performed Kirchhoff depth migration. We observe that the new FWI velocity model improves the flatness of the offset gathers as shown in Figures 5a and 5b.

In a second example, we show results for a wide-azimuth dual-sensor dataset acquired in deep-water Gulf of Mexico with maximum inline and crossline offsets of 7km and 4.2km, respectively. Figures 6a and 6b show depth slices (1440m and 1620m) of the initial velocity model computed from reflection tomography. We perform FWI from this model using the dynamically weighted velocity kernel within a frequency bandwidth of 3-5 Hz. For the extrapolation of the wavefields, we use the pseudo-analytical method assuming a TTI medium with variable density. Figures 6c and 6d show the corresponding slices for the inverted model. As observed, the new gradient allows updates to resolve small-scale lateral heterogeneities in the velocity model, provided mainly by the presence of

A robust FWI gradient for high-resolution model building

diving waves. At the same time, there is no migration imprint in the updates produced by the specular reflections as observed in the vertical profiles for the starting and the inverted velocity models (Figures 7a and 7b). Finally, in Figures 8a and 8b, we show sample image gathers computed from the starting and inverted velocity model, respectively. These illustrate the improvement in the flatness of the gathers after inversion.

Conclusions

We describe a new robust solution for recovering the long-wavelength features of a velocity model in gradient-based FWI. The method uses reflected and transmitted wave modes to recover high-resolution velocity models. The new FWI gradient enables reliable velocity updates deeper than the maximum penetration depth of diving waves, and reduces the FWI dependency on recording ultra-long offsets.

Acknowledgments

We thank PGS for permission to publish the results. We thank Dan Whitmore and Lingyun Qiu for helpful discussions.

Figure 1. Sensitivity kernels of a source-receiver pair in a model with a homogeneous layer overlying a half-space: (a) bulk-modulus, (b) density, (c) impedance and (d) velocity.
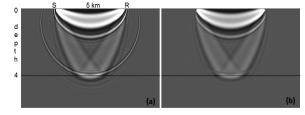

Figure 2. Sensitivity kernels of a source-receiver pair in a model with a V(z) layer overlying a half-space: (a) conventional kernel and (b) velocity kernel.
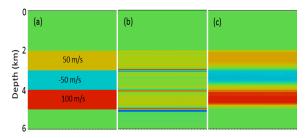

Figure 3. Five layer synthetic model: (a) Difference between exact and starting model, and between the inverted and the initial velocity model using the (b) conventional and (c) new FWI gradients.
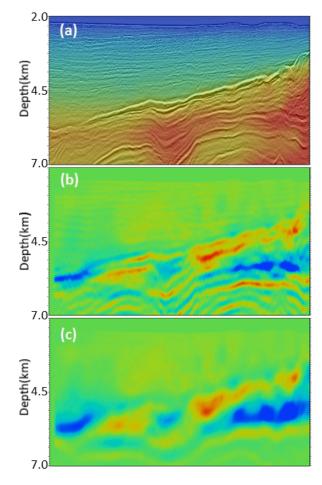

Figure 4. 2D dual sensor data example from deep-water Gulf of Mexico: (a) initial velocity model overlaid by the seismic image, (b) conventional FWI model update and (c) new FWI model update.

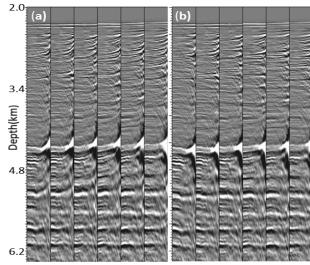# A robust FWI gradient for high-resolution model building

Figure 5. Kirchhoff offset gathers from the (a) initial and (b) inverted velocity model using the dynamically weighted gradient, corresponding to the 2D Gulf of Mexico example.
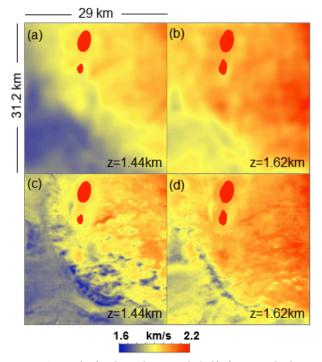

Figure 6. Results for the wide-azimuth Gulf of Mexico dual-sensor data example using the dynamically weighted gradient: Initial (a and b) and inverted (c and d) velocity model slices corresponding to depths 1.44 km and 1.62km.
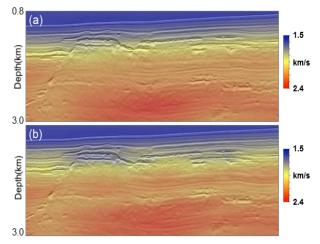

Figure 7. Results for the wide-azimuth Gulf of Mexico dual-sensor data example using the dynamically weighted gradient: Vertical profiles for the (a) starting and the (b) inverted velocity model overlaid by the corresponding migrated stacked images. Horizontal distance is 16.5 km.
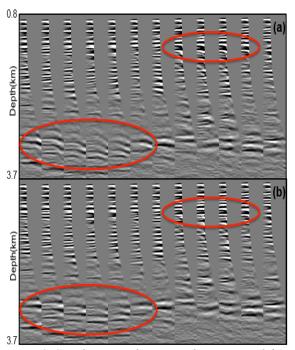

Figure 8. Sample migrated image gathers computed from the (a) starting and (b) inverted velocity model for the wide-azimuth Gulf of Mexico data example. Improvements in the flattening of the gathers are highlighted.

REFERENCES

Baumstein, A., W. Ross, and S. Lee, 2011, Simultaneous source elastic inversion of surface waves: 73rd
    Conference and Exhibition, EAGE, Extended Abstracts, C040.
Lazaratos, S., I. Chikichev, and K. Wang, 2011, Improving the convergence rate of full wavefield
    inversion using spectral shaping: 81st Annual International Meeting, SEG, Expanded Abstracts,
    2428–2432, http://dx.doi.org/10.1190/1.3627696.
Lu, R., S. Lazaratos, K. Wang, Y. H. Cha, I. Chikichev, and R. Prosser, 2013, High-resolution Elastic
    FWI for Reservoir Characterization, 75th Conference & Exhibition incorporating, EAGE,
    Expanded Abstracts, Th 10-02.
Plessix, R. E., 2009, Three-dimensional frequency-domain full-waveform inversion with an iterative
    solver: Geophysics, **74**, no. 6, WCC149–WCC157, http://dx.doi.org/10.1190/1.3211198.
Routh, P., J. Krebs, S. Lazaratos, A. Baumstein, I. Chikichev, N. Downey, S. Lee, D. Hinkley, and J.
    Anderson, 2011, Full-wavefield inversion of marine streamer data with the encoded simultaneous
    source method: 73rd Conference and Exhibition, EAGE, Extended Abstracts, F032.
Sirgue, L., O. I. Barkved, J. Dellinger, J. Etgen, U. Albertin, and J. H. Kommendal, 2010, Full waveform
    inversion: The next leap forward in imaging at Valhall: First Break, **28**, 65–70.
Tarantola, A., 1984, Inversion of seismic reflection data in the acoustic approximation: Geophysics, **49**,
    1259–1266, http://dx.doi.org/10.1190/1.1441754.
Vigh, D., B. Starr, J. Kapoor, and H. Li, 2010, 3D full waveform inversion on a GOM WAZ data set:
    80th Annual International Meeting, SEG, Expanded Abstracts, 957–961,
    http://dx.doi.org/10.1190/1.3513935.